Heliyon 10 (2024) e31667

Contents lists available at ScienceDirect

Heliyon

journal homepage: www.cell.com/heliyon

Research article

Metabolomics reveals that ferroptosis participates in bisphenol A-induced testicular injury

Ling Kan Chi [a,1], Qing Yuan [b,1], Min Yan Wang [c], Chun Rong Guo [d], Xian Dan Zhu [e], Hua Bo Jiang [b], Qin Hua Zhang [a], Yuan Zhao [e,**], Li Li [a,*], Hua Yan [a,***]

[a] Reproductive Medicine Center, Shuguang Hospital Affiliated to Shanghai University of Traditional Chinese Medicine, Shanghai, 201203, China
[b] Department of Gynecology, Department of Fetal Medicine and Prenatal Diagnosis Center, Shanghai First Maternity and Infant Hospital, School of Medicine, Tongji University, Shanghai, 201203, China
[c] Department of Pathology, Shuguang Hospital Affiliated to Shanghai University of Traditional Chinese Medicine, Shanghai, 201203, China
[d] Teaching Experimental Center, Shanghai University of Traditional Chinese Medicine, Shanghai, 201203, China
[e] Laboratory Animal Center, Shanghai University of Traditional Chinese Medicine, Shanghai, 201203, China

ARTICLE INFO

Keywords:
Bisphenol A
Testicular toxicity
Metabolomics
Ferroptosis
Mitochondrial damage

ABSTRACT

Objective: Bisphenol A (BPA) is a common environmental endocrine disruptor that negatively impairs male reproductive ability. This study aimed to explore the alterations in serum metabolomics that occur following BPA exposure and the mechanism via which BPA induces the death of testicular cells in a male mouse model.

Methods: The mice were classified into two groups: BPA-exposed and control groups, and samples were collected for metabolomic determination, semen quality analysis, electron microscopy, enzyme-linked immunosorbent assay, quantitative real-time PCR, pathological staining, and Western blot analysis.

Results: BPA exposure caused testicular damage and significantly decreased sperm quality in mice. Combined with non-target metabolomic analysis, this was closely related to ferroptosis induced by abnormal metabolites of arachidonic acid and phosphatidylcholine, and the expression of its related genes, acyl CoA synthetase 4, glutathione peroxidase 4, lysophosphatidylcholine acyltransferase 3, and phosphatidylethanolamine-binding protein 1 were altered.

Conclusion: BPA induced ferroptosis, caused testicular damage, and reduced fertility by affecting lipid metabolism in male mice. Inhibiting ferroptosis may potentially function as a therapeutic strategy to mitigate the male reproductive toxicity induced by BPA.

Abbreviations: BPA, bisphenol A; WB, western blot; ROS, reactive oxygen species; GPX4, glutathione peroxidase 4; Nrf2, nuclear factor erythroid 2-related factor 2; PE, phosphatidylethanolamine; AA, arachidonic acid; PBS, phosphate-buffered saline; H&E, Hematoxylin and eosin; UPLC-Q-TOF/MS, ultra-high performance liquid chromatography-quadrupole time-of-flight mass spectrometry; VIP, variable importance in the projection; MeV, Multi Experiment Viewer; MDA, malondialdehyde; PC, phosphatidylcholine; PGG2, prostaglandin G2; GAPDH, glyceraldehyde-3-phosphate dehydrogenase; ANOVA, analysis of variance; OPLS-DA, orthogonal partial least squares discriminant analysis; PUFAs, polyunsaturated fatty acids; ACSl4, acyl-CoA synthetase long-chain family member 4; LPCAT3, lysophosphatidylcholine acyltransferase3; LOX, lipoxygenase; PEBP1, phosphatidylethanolamine binding protein 1; GSH, glutathione.

* Corresponding author.
** Corresponding author.
*** Corresponding author.
E-mail addresses: cmx_1@126.com (Y. Zhao), lili-doublelee@hotmail.com (L. Li), 13524658288@163.com (H. Yan).
[1] Ling Kan Chi and Qing Yuan contributed equally to this work.

https://doi.org/10.1016/j.heliyon.2024.e31667
Received 5 October 2023; Received in revised form 20 May 2024; Accepted 20 May 2024
Available online 23 May 2024

1. Introduction

Bisphenol A (BPA) is an environmental endocrine disruptor. It is widely utilized as a raw material for synthesizing polycarbonate and epoxy resins in manufacturing goods that humans frequently use. Humans are frequently exposed to BPA pollution daily, and the body mainly absorbs BPA through the digestive tract and skin contact. Previous studies have reported BPA in many adult blood, urine, and adolescent male urine samples [1]. BPA causes various endocrine diseases, including infertility, precocious puberty, hormone-dependent tumors, and metabolic diseases such as polycystic ovary syndrome. Among metabolic diseases, type 2 diabetes is of great concern, and BPA exposure can lead to insulin resistance, which affects glucose metabolism [2]. BPA induces apoptosis through caspase activation after mitochondrial injury and impairs the insulin signaling pathway by altering potassium channels, leading to a series of metabolic disorders [3]. Among them, damage to male reproductive function mainly manifests as a reduction in testicular weight and epididymal sperm quantity, a decrease in serum testosterone levels, and changes in spermatogenesis [4]. Research has demonstrated that BPA-induced damage to the male reproductive system involves testicular cell death, ultrastructural destruction, and spermatogenic dysfunction [5,6]. Previous studies have shown that ferritinophagy is involved in BPA-induced ferroptosis of renal tubular epithelial cells through the activation of the AMPK-mTOR-ULK1 pathway and that BPA induces placental ferroptosis via the YAP/TAZ-ferritinophagy axis [7,8]. Nevertheless, the comprehensive mechanism by which BPA causes testicular cell death *in vivo* via a series of biochemical reactions remains unclear. Recent studies have shown that BPA-induced reproductive toxicity is related to oxidative stress, apoptosis, blood-testicular barrier disruption, and dysregulation of fatty acid metabolism [9–12].

Dixon initially identified a new type of programmed cell death called ferroptosis in 2012, which has an obvious iron dependence, and its biochemical, morphological, and genetic features differ from apoptosis, autophagy, and pyroptosis. Biochemically, the depletion of intracellular glutathione (GSH), the reduction in the activity of glutathione peroxidase 4 (GPX4), the inability of lipid peroxides to be processed by reduction reactions mediated by GPX4, and the oxidation of lipids by ferric iron in a Fenton reaction produces large amounts of reactive oxygen species (ROS) [13]. Morphologically, ferroptosis occurs mainly within the cell, with a decrease in the volume of mitochondria, as well as an increase in the density of the membrane, and a blurred, reduced, or absent mitochondrial crest, but normal-sized nuclei and an intact cell membrane are observed. Genetically, ferroptosis mainly involves genetic alterations of ferroptosis and lipid peroxidation, and numerous genes regulate the process of death. The contribution of ferroptosis in numerous pathophysiological processes, including cancer, liver fibrosis, and cardiovascular disease, has extensively been reported [14–16]. Ferroptosis has been linked to male reproductive dysfunctions, according to recent research. The inhibition of ferroptosis increases sperm concentration and motility in nuclear factor erythroid 2–related factor 2 (Nrf2) knockout mice [17]. Nevertheless, the precise link between testicular injury induced by BPA and ferroptosis is still uncertain.

Metabolomics is a research method for quantitatively analyzing metabolites (such as amino acids, lipids, and sugars) in biological fluids or tissues, which can reveal the dynamic changes in metabolites. Many studies have clarified the pathogenesis of diseases through joint research on metabolomics and molecular biology, which also provides technical support for a deeper comprehension of the potential and complex biological mechanisms of human disease pathogenesis. A previous study has shown that after the body absorbs BPA, it leads to a series of metabolic disorders, and long-term exposure to BPA changes the corresponding enzymatic and metabolic pathways; thus, disturbing normal carbohydrate and lipid metabolic activities [18]. Diamante et al. [19] studied mice subjected to low doses of BPA during prenatal development. The study revealed disturbances in peroxisome proliferator-activated receptors, fatty acid metabolism, oxidative phosphorylation, and mammalian target of rapamycin signaling pathways in offspring male mice. A metabolomics study revealed that BPA changed the composition of n-6 fatty acid and decreased antioxidant enzyme levels in rat testes [9]. Moreover, the accumulation of polyunsaturated fatty acid oxides is a distinguishing feature of ferroptosis. Within this process, phosphatidylethanolamine (PE)-containing arachidonic acid (AA) or its derivative, epinephrine, plays a significant function as a lipid oxidase that induces ferroptosis [20,21] Nevertheless, metabolomics-based publications regarding the involvement of ferroptosis in testicular injury induced by BPA are scarce.

Therefore, this study aimed to explore metabolic perturbations of endogenous compounds at the metabolic level, without any specific hypothesis, using non-targeted metabolomics technology in experimental animal models. By exploring whether the mechanism via which BPA induces testicular injury involves ferroptosis influenced by metabolomics, we hope to understand the possible mechanistic basis of testicular injury induced by BPA and offer novel therapeutic strategies for combating the reproductive toxicity induced by BPA.

2. Material and methods

2.1. Experimental animal

A total of twenty male Institute of Cancer Research (ICR) mice, all of which were 8 weeks old, weighing 20–25 g, and specific pathogen-free (SPF), were procured from the Experimental Animal Center of the Shanghai University of Traditional Chinese Medicine (Shanghai, China). The ambient temperature and humidity were controlled, and a 12-h light/dark cycle (lights off at 19:00) was maintained with unrestricted water and food. All experimental animal protocols were conducted according to the NIH guidelines and approved by the Shanghai University of Traditional Chinese Medicine's Experimental Animal Ethics Committee on November 29, 2021 (PZSHUTCM211129022).

2.2. Establishment of mouse models

After adaptive feeding, two groups (n = 10 per group) of mice were established at random, control, and BPA groups. After dissolving BPA (Sigma Aldrich, St. Louis, MI, USA) in pure olive oil (BBI, SANGON Biotech Co., Ltd., Shanghai, China), it was mixed at concentrations of 0 and 100 mg/kg. Mice in each group were intragastrically gavaged once daily for 45 days. After administration, the materials were collected according to the experimental objectives to complete subsequent experiments.

2.3. Epididymal sperm analysis

Mice from both groups had their epididymal tails minced and placed in 0.5 ml G-IVF plus solution (Vitrolife Sweden AB, Goteborg, Sweden) pre-warmed at 37 °C for half an hour. Subsequently, sperm from the epididymis was extracted by collecting the upper portion of the suspension. A Makler counting plate was added with 20 μL of sperm suspension dropwise, and the suspension was analyzed with a computer-assisted sperm analysis system (CASA) (Beijing Weili Co., Ltd., Beijing, China). To ascertain the concentration and motility of the sperm, 10 regions were captured for every sample. In addition, the sperm solution was diluted and then a drop was put onto a glass slide, and the slide was pushed. After drying, we performed a modified PAP staining technique and examined the sperm morphology under the oil microscope. We analyzed 200 sperm in a continuous field and calculated the deformity rate.

2.4. Sperm morphology observed by scanning electron microscopy

After centrifugation had been conducted at 8000 rpm for half an hour, the supernatant was discarded, fixed with 2 % glutaraldehyde for 3 h, rinsed thrice using 0.1 M phosphate-buffered saline (PBS), centrifuged at 8000 rpm at 4 °C for half an hour each time, fixed for 3 h with 1 % osmic acid, washed thrice using 0.1 M PBS, centrifuged at 8000 rpm at 4 °C for half an hour each time, and dehydrated with graded alcohol. The sperm were collected at a pore size of 0.4 μM polycarbonate film, placed into a critical point dryer (Leica cpd 300, Germany) for drying, and an ion sputtering instrument (Leica EM ace 600, Leica Microsystems, Austria) was used for surface gold plating, and finally, a scanning electron microscope (Quanta FEG 250, Philips, the Netherlands) was used to observe the sperm.

2.5. Hematoxylin and eosin (H&E) staining of testicular tissue

Following fixation in Bouin's solution, the testicular tissues were embedded in paraffin and sectioned. Conventional dewaxing and rehydration were then performed. Hematoxylin (Harris) dye solution (BASO, Zhuhai Beisuo Biotechnology Co, Ltd, China) was applied for 40 s, washed with running water, differentiated for 5 s with 1 % hydrochloric acid alcohol, rinsed using running water, exposed to 1 % ammonia solution back to blue for 60 s, washed with running water, stained with eosin dye (BASO) for 10 s, rinsed using running water, dehydrated, made to be transparent, and sealed for microscopic observation.

2.6. PAS hematoxylin staining of testicular tissue

Testicular tissue was fixed in Bouin's solution, and after routine paraffin embedding, sectioning, dewaxing, and rehydration, periodic acid solution (BASO) was oxidized for 40 min, washed using running water, stained with Schiff reagent (BASO) for 40 min, washed using running water, stained with hematoxylin (BASO) for 2 min, washed using running water for 3 min, dehydrated, made to be transparent, and sealed for microscopic observation. In round spermatids, the reddish sections indicate a positive staining reaction, specifically highlighting the acrosome cap. When examining stage VIII seminiferous tubules under the microscope, it can be observed that the acrosomal cap of most round spermatids points to the seminiferous tubule basement membrane. This orientation signifies spermiation, where the elongated spermatids are released as mature spermatozoa into the lumen [22]. The proportion of stage VIII seminiferous tubules was calculated.

2.7. Mitochondrial morphology observed using transmission electron microscopy

The testicular tissue sample was divided into 1 mm^3 small pieces on ice with a disposable double-sided blade, fixed in 2.5 % glutaraldehyde, and stored at 4 °C. The samples underwent dehydration in a gradient of acetone and ethanol, followed by embedding in paraffin. Lead citrate-stained ultrathin sections measuring 70 nm in thickness were prepared using this approach. A transmission electron microscope (Fei TECNAI G2 Spirit; Thermo Fisher Scientific, Waltham, Ma, USA) was utilized to observe the morphology, quantity, and ultrastructure of the mitochondria.

2.8. Serum sample metabolomics profiling

An ultra-high pressure liquid chromatography (UHPLC) system (1290 Infinity LC, Agilent Technologies) coupled to a quadrupole time-of-flight (AB SCIEX Triple TOF 6600), was utilized as instructed by Shanghai Applied Protein Technology Co., Ltd (Shanghai, China) to analyze untargeted metabolomics profiling of serum samples. The conditions for electrospray ionization sources and the product ion scan were set following the parameters indicated by Zhou et al. [23].

The Proteo Wizard MS converter program was used to transform the raw UPLC-Q-TOF/MS data into mzXML files, which were

further analyzed utilizing the web-based XCMS software [24]. The metabolites were subjected to characterization through the comparison of their fragmentation patterns, retention times, and m/z values (<25 ppm) with an in-house database that had been created utilizing publicly accessible authentic standards [23]. Univariate Student's t-test was employed to assess the significance of individual metabolites that possessed variable importance in the projection (VIP) values > 1, utilizing the Benjamin–Hochberg procedure to account for multiple testing and setting the critical false discovery rate to 0.05. After the implementation of unit variance scaling for each metabolite, a heat map of the metabolites was generated utilizing the Multi Experiment Viewer (MeV) software 4.9.0.

2.9. Determination of malondialdehyde (MDA), ferritin, phosphatidylcholine (PC), prostaglandin G2 (PGG2), OXPC, and AA in testicular tissues

To aspirate the supernatant, 30 mg of mouse testis tissues were mixed with 300 μL of normal saline, which then underwent homogenization on ice and was centrifuged at 4 °C for 10 min at 1000 rpm. Following the guidelines provided in the BSA Kit (Beyotime, Shanghai, China), we prepared a standard solution and added it to the 96-well enzyme plate along with the sample. We allowed the mixture to react at 37 °C for 30 min, measured the absorbance value of the samples at the wavelength of 562 nm, and calculated the protein concentration. Subsequently, we followed the procedural instructions outlined in the mouse ferritin enzyme-linked immunosorbent assay Kit (Shanghai Shenzhen Biotechnology Co, Ltd, China). We prepared the standard solution and added the samples to a 96-well enzyme standard plate. Following the completion of incubation, plate washing, and color development, we used a colorimetric analyzer (Thermo Multiskan FC, Waltham, Ma, USA) to measure the absorbance value of the samples at 580 nm. Finally, the concentration of each index was measured.

2.10. Immunohistochemical analysis

Following fixation in Bouin's solution, paraffin embedding, and sectioning, the testicular tissues were subjected to routine dewaxing and rehydration. Then, antigens were retrieved by heating the slides in citrate buffer (pH 6.0) at 98 °C for half an hour and cooling them naturally. Following blocking with nonspecific antigens and inactivating endogenous peroxidase, the cells were allowed to incubate at 4 °C for 12 h with the primary antibody. The sources of antibodies source and their respective dilutions were as follows: GPX4 (1:1000, Proteintech, Sanying Biotechnology Co., Ltd., Wuhan, China), ACSl4 (1:100, Proteintech), LPCAT3 (1:200, Proteintech), PEBP1 (1:300, Proteintech). After rinsing the slides using PBS, the tissue sections were subjected to incubation for half an hour with corresponding secondary antibodies (Proteintech) at 25 °C. Thereafter, the diaminobenzidine (DAB) chromogenic liquid was added to the slides for color development. Then, images were captured using a microscope (Olympus bx53; Olympus, Tokyo, Japan) fitted with a digital camera (Olympus dp73, Olympus). The positive expression was denoted by the tanned area, and Image-Pro Plus 6.0 (Media Cybernetics, Inc., Bethesda, MD, USA) was utilized to estimate the "density (mean)" of the average staining intensity.

2.11. Quantitative real-time PCR (qRT-PCR)

Testicular tissues were washed in cold PBS, and TRIzol reagent (BBI, SANGON Biotech Co., Ltd., Shanghai, China) was utilized for the extraction of total RNA, followed by quantification and reverse-transcription of total RNA utilizing a first-strand cDNA synthesis kit (Takara Bio Inc., Beijing, China). SYBR® Premix TB Green Premix Ex Taq (Takara Bio Inc., China) was adopted for qRT-PCR to detect the expression of GPX4, ACSL4, LPCAT3, and PEBP1. All primer sequences are presented in Table 1. The target genes' relative expression was normalized utilizing the average level of glyceraldehyde-3-phosphate dehydrogenase (GAPDH). Subsequently, the relative gene expression level was calculated using the $2^{-\Delta\Delta CT}$ method.

2.12. Western blot

After extracting and separating the total sperm protein using 12 % sodium dodecyl-sulfate polyacrylamide gel, they were transferred onto a polyvinylidene fluoride (PVDF) membrane. Skimmed milk was added to block the membranes for 2 h, after which they were subjected to incubation at 4 °C for the night with primary antibodies GPX4 (1:2000, Proteintech), ACSL4 (1:2000, Proteintech),

Table 1
Primer sequences.

Genes	Primer sequences (5′–3′)	Amplicon
Gapdh	Forward: AGGTCGGTGTGAACGGATTTG Reverse: TGTAGACCATGTAGTTGAGGTCA	123
Gpx4	Forward: GATGGAGCCCATTCCTGAACC Reverse: CCCTGTACTTATCCAGGCAGA	185
Acsl4	Forward: CTCACCATTATATTGCTGCCTGT Reverse: TCTCTTTGCCATAGCGTTTTTCT	114
Lpcat3	Forward: CTACCCGTTGGCTCTGTTTTAC Reverse: TGAAGCACGACACATAGCAAG	147
Pebp1	Forward: ACAATCGCGGCAAGTTCAAG Reverse: TGGGCACATAGTCATCCCACT	105

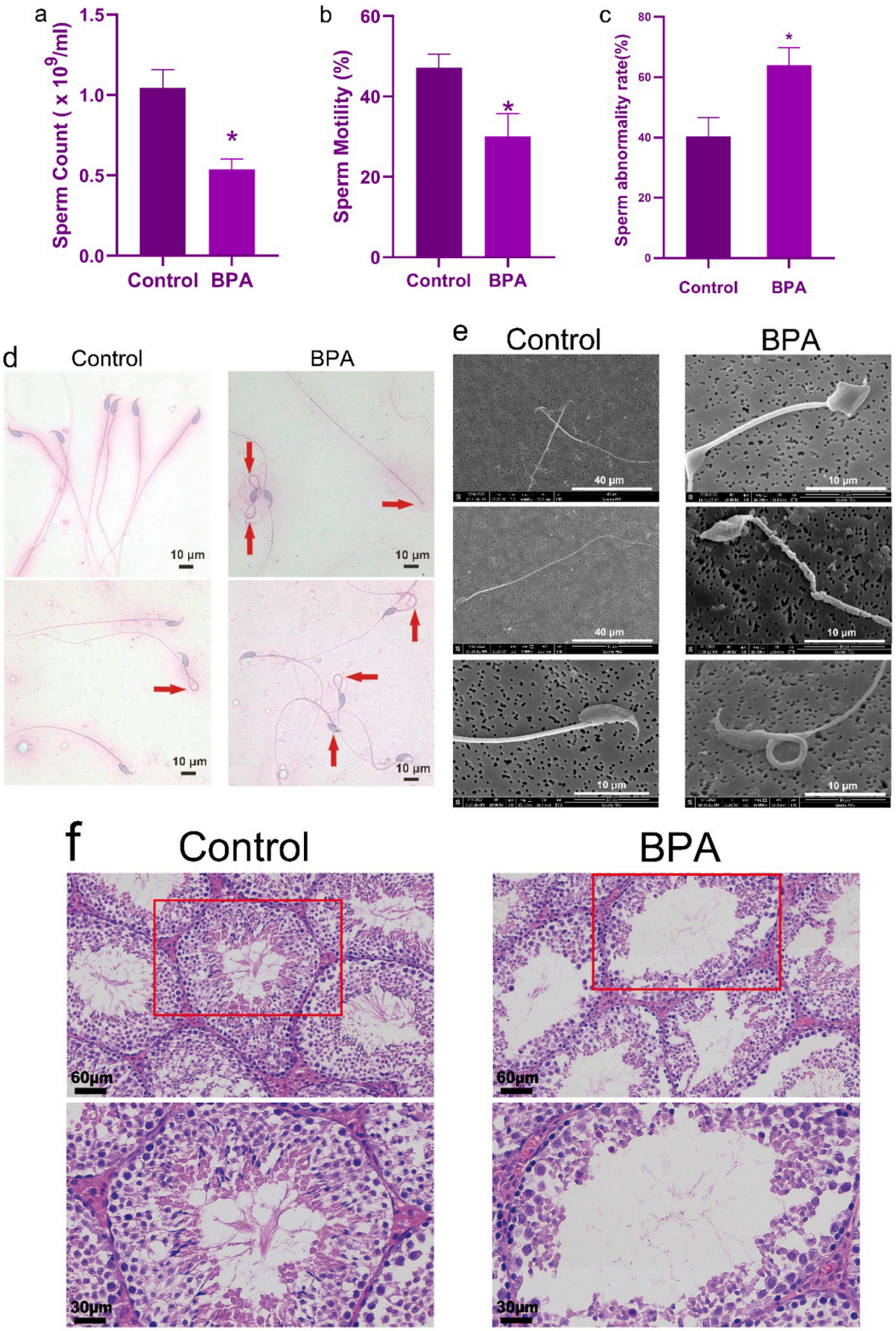

Fig. 1. Bisphenol A exposure causes pathological damage to testicular tissues and decreases sperm quality in mice.
a. Comparison of epididymal sperm concentrations. b. Comparison of epididymal sperm viability. c. Comparison of sperm deformity rates in the epididymis. d. Abnormal sperm (modified PAP staining), including head deformities, neck curvatures, and headless sperm, were observed under an oil microscope. Scale bar = 10 μm. (e) Sperm morphology was observed under a scanning electron microscope. Scale bar = 40 and 10 μm. f.

Testicular tissues stained with hematoxylin and eosin (H&E). Scale bar = 60 and 30 μm. (g) PAS hematoxylin staining. Scale bar = 30 μm. Values are expressed as the mean ± S.D. of three independent experiments *Statistically significant difference compared to the control group ($P < 0.05$); S.D.: Standard deviation.

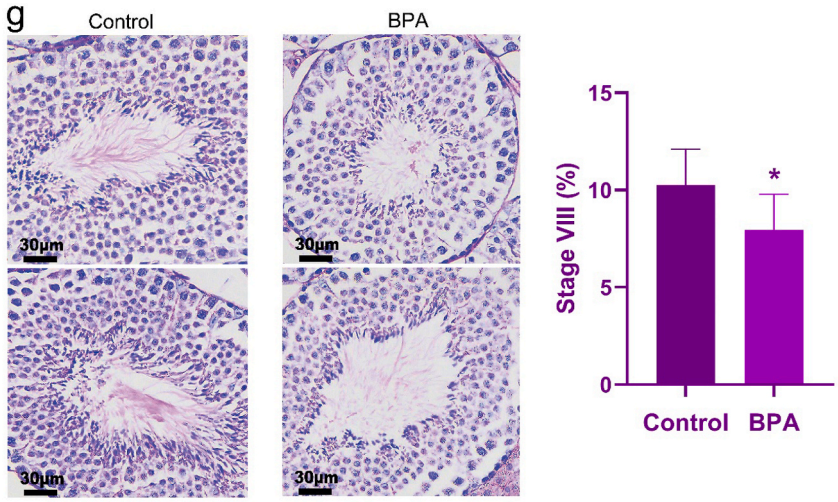

Fig. 1. (*continued*).

LPCAT3 (1:1000, Proteintech), and PEBP1 (1:1000, Proteintech). The following day, the secondary antibody was blocked with shaking for 2 h at ambient temperature. The samples were processed and visualized in a Ge Amersham imager 600 machine (GE Healthcare Bio-Sciences Corp., Piscataway, NJ, USA), and semi-quantitatively analyzed with β-actin as an internal reference.

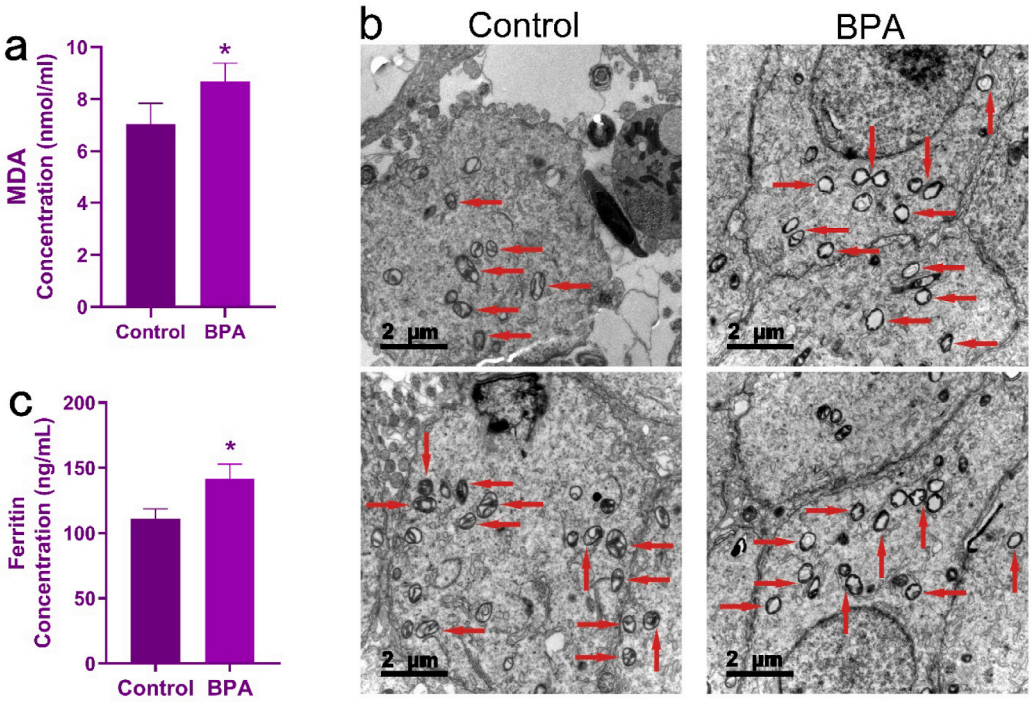

Fig. 2. Bisphenol A exposure resulted in oxidative damage and accumulation of iron in the mouse testes.
a. Comparison of MDA concentrations in testicular tissues between the two groups. b. A transmission electron microscope was used to visualize the morphology of the mitochondria in the testis tissue of the two groups of mice. Scale bar = 2 μm. c. Comparison of ferritin concentration in testicular tissues between the two groups. Values are expressed as the mean ± S.D. of three independent experiments *Statistically significant difference compared to the control group ($P < 0.05$); S.D.: standard deviation; MDA: malondialdehyde.

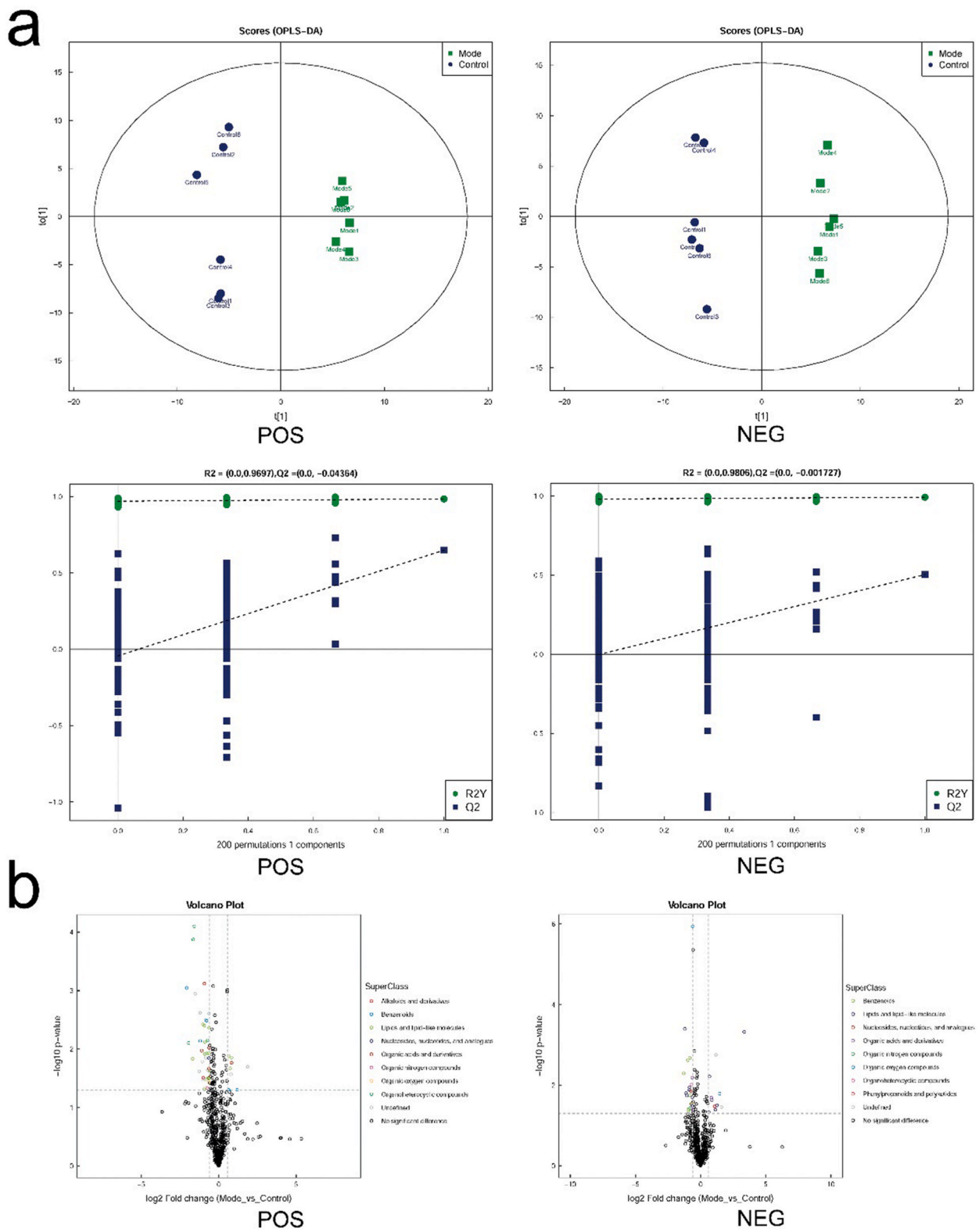

Fig. 3. Bisphenol A exposure altered the serum metabolic profiles of mice.
a. Positive and negative ion modes of serum metabolic profiles are shown using the OPLS-DA score plot. b. The screening of differential metabolites under positive and negative ion modes and a volcano map of serum metabolic characteristics were drawn after the classification of chemical

substances. c. Clustering Heatmap of negative and positive ion modes of differential serum metabolite. d. The bar chart shows the fold-change in lipids in the identified significantly different metabolites.

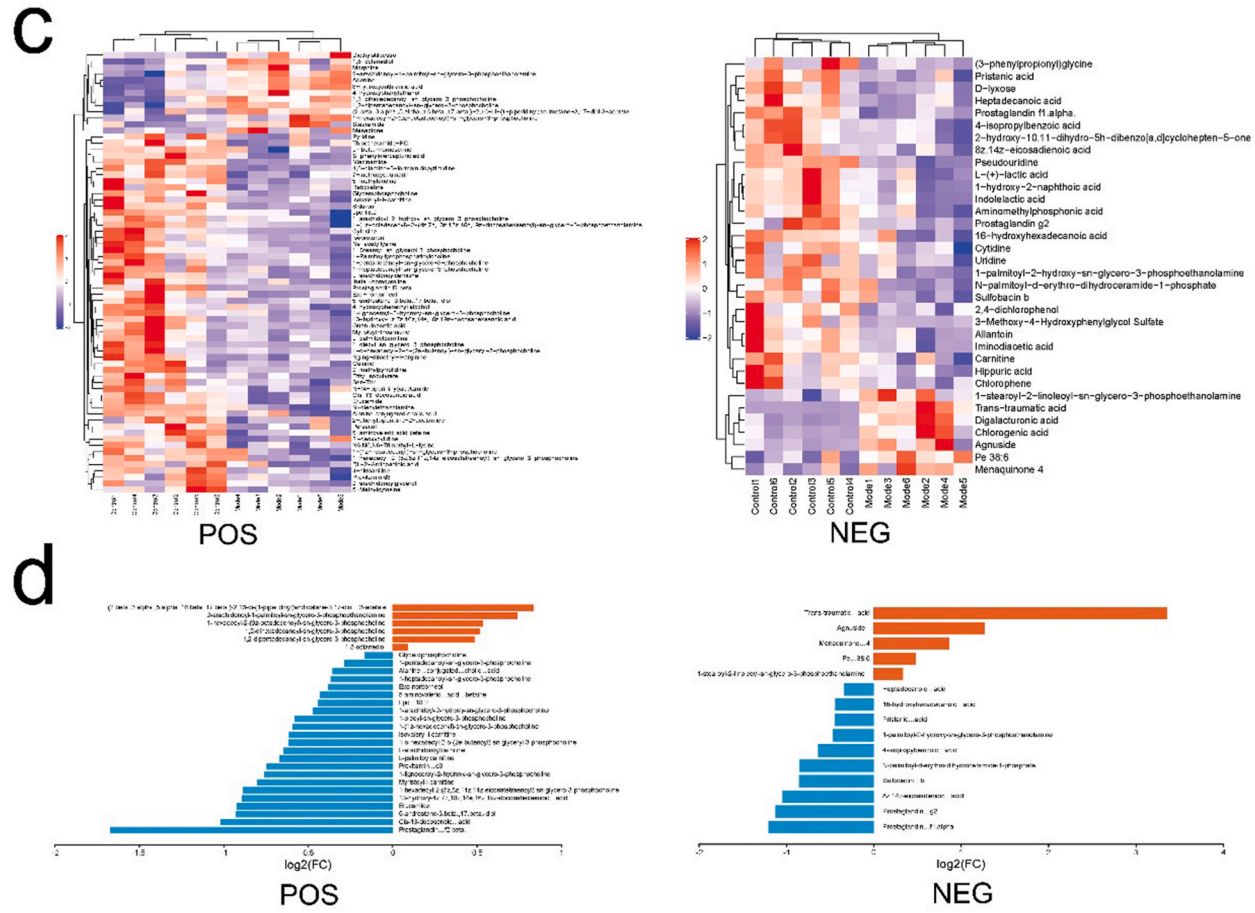

Fig. 3. (*continued*).

2.13. Statistical analysis

SPSS software (v 21.0; IBM, Armonk, NY, USA) was utilized to analyze the statistical data, and results were presented using mean ± standard deviation. Comparative analysis across various groups was accomplished utilizing a one-way analysis of variance (ANOVA), and the LSD method was applied for pairwise comparisons. $P < 0.05$ indicated significant differences.

3. Results

3.1. Bisphenol-A exposure induced pathological damage of testicular tissue and decreased sperm quality in mice

The epididymal sperm were observed and analyzed after 45 days of gavage administration of BPA (100 mg/kg) to the mice. Both the quantity and quality of sperm were significantly reduced in the treated group relative to the control ($P < 0.05$, Fig. 1a and b). An oil microscope was employed to examine the morphology of the sperm. The number of sperms with head deformity, tail deformity, and headless sperm in the BPA group was significantly higher than that in the control mice (Fig. 1C and d) ($P < 0.05$). Sperm morphology was observed using scanning electron microscopy, and different degrees of head deformity, neck bending, swelling, and roughneck surface were observed (Fig. 1e). We further observed the pathohistology of mouse testes and found that under BPA exposure, the spermatogenic cells of mouse testes were widened and arranged disorderly, the number of layers was reduced, the structure was unclear, and the count of sperm in the lumen of the seminiferous tubules was decreased (Fig. 1f). Simultaneously, PAS hematoxylin staining showed that the number of seminiferous tubules in stage VIII in the BPA group was significantly reduced relative to the control group ($P < 0.05$) (Fig. 1g); spermatogenesis was also affected to a certain extent.

3.2. Exposure to BPA in mice resulted in oxidative damage and accumulation of iron in the testis

We analyzed the MDA level in mouse testis tissue to determine the causes of the pathological damage to the testis and the low quality of sperm in mice induced by BPA exposure. We found that MDA concentration was significantly increased in the BPA group in comparison to that in the control mice ($P < 0.05$) (Fig. 2a). The ultrastructure of the mouse testicular cells was observed using transmission electron microscopy. Notably, BPA treatment significantly damaged the mitochondria in testicular cells, including mitochondrial membrane pyknosis, increased membrane density, mitochondrial swelling, rounding, breakage or disappearance of mitochondrial cristae, and rupture of the outer membrane (Fig. 2b). Simultaneously, the observed mitochondrial damage in testicular cells was similar to the typical morphological changes of cell ferroptosis; therefore, we analyzed the ferritin concentration in testicular tissues to further confirm this view and found a significant increase in ferritin in the group exposed to BPA relative to the control mice ($P < 0.05$) (Fig. 2c).

3.3. Serum metabolomic changes induced by BPA exposure in mice

We analyzed the metabolic perturbations produced by BPA and the alterations in serum metabolites in mice utilizing non-target metabolomics. Both the negative and positive ion modes were examined using the orthogonal partial least squares discriminant analysis (OPLS-DA) model. Serum metabolic profiles of the BPA and control mice were significantly different, according to the OPLS-DA score map (negative ion mode: $r2y = 0.992$, $q2 = 0.503$; positive ion mode: $r2y = 0.985$, $Q2 = 0.649$), indicating that the model has good adaptability and prediction ability. The OPLS-DA model showed good verifiable parameters, and a permutation test of 200 iterations proved that the model was not overfitted (Fig. 3 a). We identified 1237 metabolites (675 and 562 in the positive and negative ion modes, respectively). Additionally, fold change >1.5 or <0.67 and P value < 0.05 were employed to identify differential metabolites. Compared with the control group, the levels of 70 metabolites decreased, and the expression of 38 metabolites increased in the positive ion mode. Conversely, the levels of 34 metabolites decreased, and the expression of 13 metabolites increased in the negative ion mode. Differential metabolites were classified according to the chemical taxonomy attribution information. Among the differential metabolites are lipid molecules, alkaloids, benzene compounds, nucleotides, organic acids, organic oxygen, and organic nitrogen. (Fig. 3b). Notably, the cluster heatmap could distinguish the BPA from the control mice based on the stringent screening parameters of $P < 0.05$ and OPLS-DA VIP >1. The number of up-and down-regulated metabolites in the BPA group were 13 and 57 in the positive ion mode and 7 and 27 in the negative ion mode, respectively (Fig. 3c). Among these significantly different metabolites, we focused on the differential fold changes in lipids (Fig. 3d). We further observed that phosphatidylcholine was significantly upregulated in the positive ion mode. In contrast, PGG2 was significantly downregulated in the negative ion mode, which led to lipid peroxidation of membrane phospholipids containing phosphatidylcholine through the involvement of AA metabolism, ultimately leading to ferroptosis in BPA-exposed mice (Fig. 4). To verify the results of the biological information analysis and our hypothesis, we detected relevant indicators in the testicular tissue homogenates.

3.4. Abnormal concentration of lipid peroxidation metabolites in mice testis tissue under BPA treatment

The testicular tissue was homogenized, and PC, AA, PGG2, and OXPC were detected. The results showed a significant increase in the concentrations of PC, AA, and OXPC in the BPA group relative to the control (Fig. 5a, b, and c) ($P < 0.05$), and a decrease in PGG2 levels, but the difference was insignificant ($P > 0.05$) (Fig. 5E).

3.5. BPA exposure caused alterations in the expression of related indicators of ferroptosis under the influence of lipid metabolism pathways in mouse testis tissue

To ascertain whether ferroptosis occurred in the testicular tissue of BPA-exposed mice, we performed qRT-PCR and WB analyses

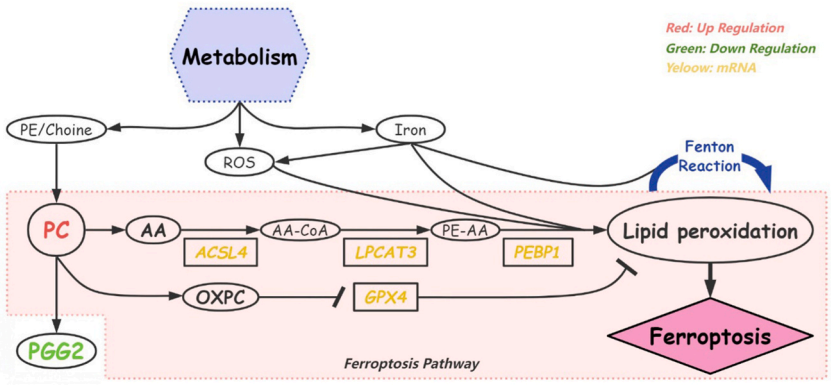

Fig. 4. Ferroptosis occurs through lipid metabolism pathways.

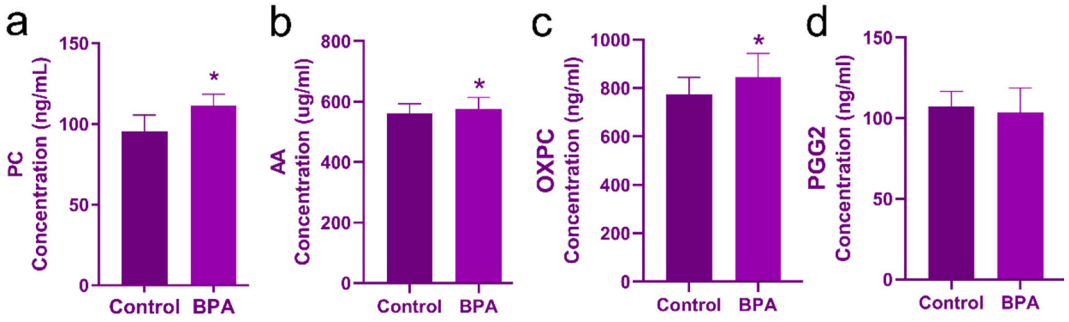

Fig. 5. The concentration of lipid peroxidation metabolites in mouse testis tissue was abnormal under bisphenol A exposure.
a. Comparison of PC concentration in testicular tissue between the two groups. b. Comparative analysis of the concentrations of OXPC in testicular tissue from the two groups. c. Comparative analysis of the concentrations of AA in testicular tissue between the two groups. d. Comparative analysis of the concentrations of PGG2 in testicular tissue between the two groups. Values are expressed as the mean ± S.D. of three independent experiments *Statistically significant difference compared to the control group ($P < 0.05$); S.D.: standard deviation; PC: phosphatidylcholine; OXPC: oxidized phosphatidylcholine; AA: arachidonic acid; PGG2: prostaglandin g2.

examining the GPX4, ACSL4, LPCAT3, and PEBP1 expression, which are indicators of ferroptosis under the influence of lipid metabolism pathways. Accordingly, the protein and mRNA expression of GPX4 was decreased ($P < 0.05$), whereas that of ACSL4, LPCAT3, and PEBP1 was increased ($P < 0.05$) in the BPA group relative to the control group (Fig. 6).

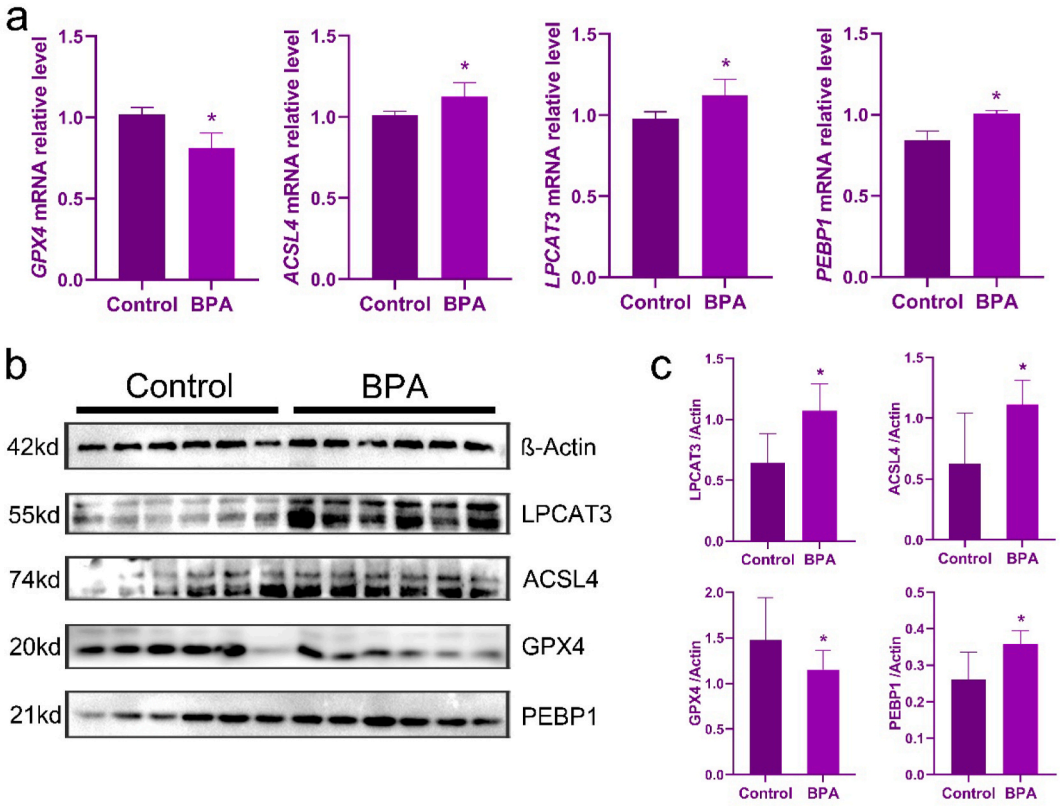

Fig. 6. Bisphenol A exposure changed the expression of related indicators of ferroptosis under the influence of the lipid metabolism pathway in mouse testis tissue.
a. The relative expression of GPX4, ACSL4, LPCAT 3 and PEBP1 mRNA. b. Levels of GPX4, ACSL4, LPCAT3, and PEBP1 were determined by Western blot. c. Protein band intensity was normalized to that of β -actin and expressed as the mean ± S. D of three independent experiments. *Statistically significant difference compared to the control group ($P < 0.05$); S.D.: standard deviation; GPX4: glutathione peroxidase 4; ACSL4: acyl-CoA synthase 4; LPCAT3: lysophosphatidylcholine acyltransferase 3; PEBP1: phosphatidylethanolamine binding protein 1; GAPDH: glycoraldehyde-3-phosphate dehydrogenase; β -Actin: beta-actin.

3.6. GPX4, ACSL4, LPCAT3, and PEBP1 expression in testis tissue

Finally, the testicular tissue's GPX4, ACSL4, LPCAT3, and PEBP1 expression levels were determined using immunohistochemistry methods. The expression of GPX4 was observed in spermatogenic cells; LPCAT3 expression was predominantly observed in spermatogenic and interstitial cells; ACSL4 and PEBP1 were expressed in spermatogenic, interstitial, and Sertoli cells. Notably, a significant decrease in GPX4 expression was observed in the BPA group relative to the control, and a significant variation was observed in the mean density between the two groups ($P < 0.05$). Conversely, the BPA group exhibited a significant reduction in ACSL4, LPCAT3, and PEBP1 expression in the BPA group in comparison to the control group, with a significant difference in the mean density ($P < 0.05$) (Fig. 7). The findings correspond with the results obtained from both the qRT-PCR and WB analysis.

4. Discussion

BPA has significant reproductive toxicity, and its effects on male reproduction can vary depending on age, exposure dose, and duration, and it may be passed on to the offspring [25]. Within the scope of this research, we evaluated the features of testicular injury that occurred as a result of exposure to BPA and analyzed the mechanism of toxicity via the use of metabolomics. Notably, we found that ferroptosis, which is affected by metabolism, was associated with testicular damage induced by BPA exposure and might give rise

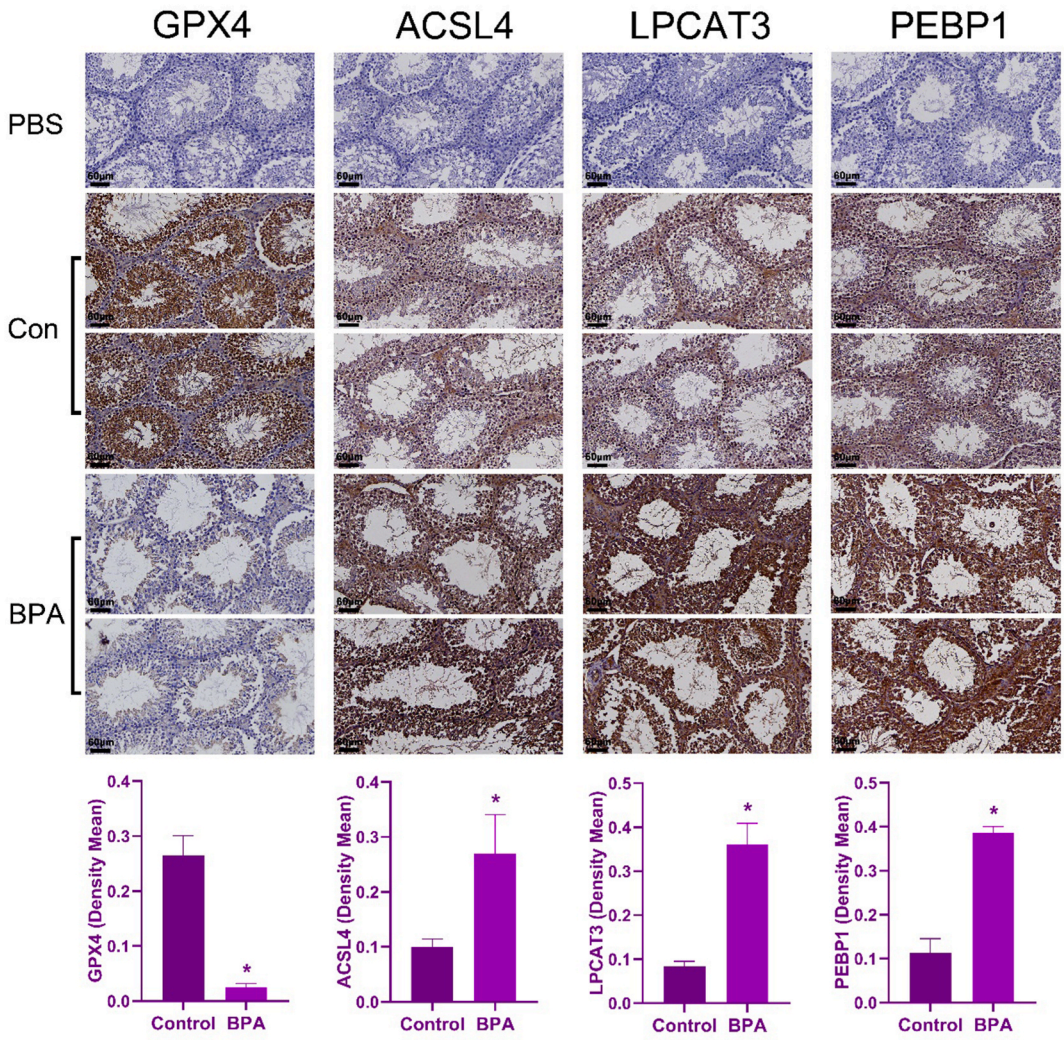

Fig. 7. Expression of GPX4, ACSL4, LPCAT3, and PEBP1 in testicular tissues.
Negative control results obtained by incubating the samples with PBS rather than primary antibody are denoted in the "PBS" column. A positive expression "Density (mean)" of the average staging intensity captured with *Image-Pro Plus 6.0* is denoted by the tan area. Scale bar = 60 μm. Values are expressed as the mean ± S.D. of three independent experiments. *Statistically significant difference compared to the control group ($P < 0.05$); S.D.: standard deviation; GPX4: glutathione peroxidase 4; ACSL4: acyl-CoA synthase 4; LPCAT3: lysophosphatidylcholine acyltransferase 3; PEBP1: phosphatidylethanolamine binding protein 1.

to a novel approach to the treatment of reproductive injuries.

Previous studies have shown that BPA induces testicular injury in male mice. To characterize testicular injury following BPA exposure, we selected a dose of BPA based on previous studies and treated ICR mice with BPA (100 mg/kg) for 45 days [26]. BPA caused testicular injury in mice, accompanied by a considerable reduction in sperm count and motility and a significant increase in the rate of malformation. Scanning electron microscopy revealed that the sperms had different degrees of head deformity, neck bending, swelling, and neck surface roughness. The testicular pathology results showed that spermatogenesis in mice was adversely affected (Fig. 1). Further analysis revealed that testicular injury was closely related to oxidative stress. This study showed that BPA-induced testicular oxidative damage in mice was mainly induced by lipid peroxidation in the mitochondria. Transmission electron microscopy (TEM) revealed that BPA exposure caused the mitochondrial membrane of the testes to shrink and increase in density, mitochondria to swell and become round, the mitochondrial crest to break or even disappear, and the outer membrane to rupture. Iron influx is increased when the mitochondrial membrane is damaged, which may further enhance the formation of ROS via Fenton reactions [27]. To confirm this, we found a significant elevation in ferritin levels in the BPA-exposed mice's testes relative to those in the control mice ($P < 0.05$) (Fig. 2). These findings suggest that BPA-induced testicular damage induced by BPA is associated with ferroptosis. Notably, iron-dependent phospholipid peroxidation is the driving force behind ferroptosis, a mechanism of cell death that performs an indispensable function in the onset and progression of organ damage. Ferroptosis has been revealed to exhibit a close link to reproductive diseases, according to recent research. One study demonstrated that patients with β-thalassemia experience hypogonadism and defects in spermatogenesis, resulting from iron accumulation in the pituitary gland and testes [28]. However, several types of biological processes are intimately connected to the sensitivity of ferroptosis. These processes include the metabolism of polyunsaturated fatty acids, iron, and amino acids, as well as the biosynthesis of coenzyme Q10, phospholipids, NADPH, and glutathione [29]. Studying ferroptosis and its regulatory mechanisms will provide novel insights into the treatment of male reproductive diseases. Therefore, we used non-target metabolomic methods to analyze metabolic perturbations and changes in serum metabolites in male mice exposed to BPA. The differential metabolites included lipids, alkaloids, benzenes, nucleotides, organic acids, organic oxygen, and organic nitrogen (Fig. 3). Lipid peroxidation is an important feature of iron-mediated death. Among these differential metabolites, we observed significant upregulation of PC and downregulation of PGG2 in the BPA group. Both PC and PGG2 are involved in the AA metabolic pathway, in which PC is catalyzed by PLA2G family proteins to generate AA, and AA is catalyzed by PGG2. Moreover, AA peroxide promotes ferroptosis [30]. We verified this in male mice and found a significant increase in the concentrations of PC, OXPC, and AA in BPA-exposed mice. Although there was a decreasing trend in PGG2 levels, the difference across the two groups was insignificant (Fig. 4). Therefore, PC, OXPC, and AA should be the focus of future studies. Some studies have shown that cardiac ischemia-reperfusion (I/R) damage causes an increase in oxidized phosphatidylcholine (OXPC) production, which in turn induces cellular ferroptosis [21]. Therefore, we hypothesized that BPA induces iron-related death by affecting lipid metabolism in male mice, causing testicular damage and reducing fertility.

The lipid peroxidation of membrane phospholipids containing polyunsaturated fatty acids (PUFAs) damages cell membranes directly, according to studies. When the mitochondrial membrane is damaged, the iron influx increases, promoting ferroptosis via the Fenton reaction. The ROS formed during this period aggravates oxidative damage [27,31]. Among various membrane phospholipids, PE, which contains AA, is the main target for lipid peroxidation. Importantly, Acyl-CoA synthetase long-chain family member 4 (ACSl4) facilitates the conversion of unbound PUFA to COA, resulting in the formation of fatty acyl-CoA esters. Human lysophosphatidylcholine acyltransferase3 (LPCAT3) subsequently incorporates these esters into the PE. Pe-aa is oxidized by lipoxygenase (LOX). For LOX to induce ferroptosis and lipid peroxidation in the membrane, PE-binding protein 1 (PEBP1) must be present [32]. In contrast, the enzyme glutathione peroxidase 4 (GPX4) normally prevents cells from undergoing ferroptosis by reducing lipid peroxides to lipid alcohols via the oxidation of glutathione (GSH). The inactivation of GPX4 leads to ferroptosis and extensive lipid peroxidation in the membrane [33] (Fig. 5). Through analysis, it was found that GPX4 expression occurred in spermatogenic cells, LPCAT3 expression occurred in spermatogenic and interstitial cells, while ACSL4 and PEBP1 were expressed in spermatogenic, interstitial, and Sertoli cells. The levels of GPX4 mRNA and protein were found to be considerably lowered following BPA exposure. Moreover, the ACSl4, LPCAT3, and PEBP1 mRNA and protein levels, which are related to the AA metabolic pathway, increased in the BPA group. The ferroptosis process in spermatogenic cells within the testes can occur through AA and OXPC pathways, while the ferroptosis of interstitial and Sertoli cells is mainly through the AA pathway (Figs. 6 and 7).

5. Conclusions

Abnormal lipid metabolism-induced ferroptosis is an important mechanism underlying testicular injury following BPA exposure. The findings of this study will aid in the search for natural inhibitors of ferroptosis and the identification of possible therapeutic targets to inhibit BPA-induced ferroptosis in lipid metabolites so as to selectively regulate ferroptosis. However, this study had some limitations. Whether ferroptosis can be inhibited by affecting lipid metabolism, for example by reducing testicular injury induced by BPA, has not been fully elucidated. On the other hand, experimental conditions on animals can only be designed to mimic those encountered by humans, but they are not the same as the actual human exposure dose and time of exposure. Therefore, further investigation of the potential mechanism of mass metabolism-induced ferroptosis in BPA-induced testicular injury is required.

Animal experiments

All experimental animal procedures were performed according to the NIH guidelines and approved by the Experimental Animal Ethics Committee of Shanghai University of Traditional Chinese Medicine on November 29, 2021 (PZSHUTCM211129022).

Funding source

This work was supported by the National Natural Science Foundation of China (No. 82205166) and the Shanghai University of Traditional Chinese Medicine (No.YYKC-2021-01-151).

CRediT authorship contribution statement

Ling Kan Chi: Writing – review & editing, Writing – original draft. **Qing Yuan:** Conceptualization. **Min Yan Wang:** Supervision, Methodology. **Chun Rong Guo:** Validation. **Xian Dan Zhu:** Software. **Hua Bo Jiang:** Methodology, Formal analysis. **Qin Hua Zhang:** Writing – review & editing, Funding acquisition. **Yuan Zhao:** Project administration. **Li Li:** Writing – original draft. **Hua Yan:** Writing – original draft, Investigation.

Declaration of competing interest

The authors declare the following financial interests/personal relationships which may be considered as potential competing interests:Li Li reports financial support was provided by National Natural Science Foundation of China. Lingkan Chi reports financial support was provided by Shanghai University of Traditional Chinese Medicine. If there are other authors, they declare that they have no known competing financial interests or personal relationships that could have appeared to influence the work reported in this paper.

Acknowledgments

We thank Prof. Xiong Lu, Prof. Min Lu, and Prof. Yi Jiang from the Experiment Center for Science and Technology of Shanghai University of Traditional Chinese Medicine (Shanghai, China) for their support.

Appendix A. Supplementary data

Supplementary data to this article can be found online at https://doi.org/10.1016/j.heliyon.2024.e31667.

References

[1] J.E. Lim, B. Choi, S.H. Jee, Urinary bisphenol A, phthalate metabolites, and obesity: do gender and menopausal status matter? Environ. Sci. Pollut. Res. Int. 27 (27) (2020) 34300–34310.
[2] M.S.H. Akash, et al., Resveratrol mitigates bisphenol A-induced metabolic disruptions: insights from experimental studies, Molecules 28 (15) (2023).
[3] M.S.H. Akash, S. Sabir, K. Rehman, Bisphenol A-induced metabolic disorders: from exposure to mechanism of action, Environ. Toxicol. Pharmacol. 77 (2020) 103373.
[4] J. Santiago, et al., Fighting bisphenol A-induced male infertility: the power of antioxidants, Antioxidants 10 (2) (2021).
[5] K. Baralic, et al., Combining in vivo pathohistological and redox status analysis with in silico toxicogenomic study to explore the phthalates and bisphenol A mixture-induced testicular toxicity, Chemosphere 267 (2021) 129296.
[6] A. Balci, et al., Histopathologic, apoptotic and autophagic, effects of prenatal bisphenol A and/or di(2-ethylhexyl) phthalate exposure on prepubertal rat testis, Environ. Sci. Pollut. Res. Int. 27 (16) (2020) 20104–20116.
[7] Y. Sun, et al., Bisphenol A induces placental ferroptosis and fetal growth restriction via the YAP/TAZ-ferritinophagy axis, Free Radic. Biol. Med. 213 (2024) 524–540.
[8] L. Bao, et al., Ferritinophagy is involved in Bisphenol A-induced ferroptosis of renal tubular epithelial cells through the activation of the AMPK-mTOR-ULK1 pathway, Food Chem. Toxicol. 163 (2022) 112909.
[9] M. Chen, et al., Bisphenol A alters n-6 fatty acid composition and decreases antioxidant enzyme levels in rat testes: a LC-QTOF-based metabolomics study, PLoS One 7 (9) (2012) e44754.
[10] Cariati, F., et al., Bisphenol a: an emerging threat to male fertility, Reprod. Biol. Endocrinol. 17 (1) (2019) 6.
[11] P. Wang, et al., Mitochondrion-mediated apoptosis is involved in reproductive damage caused by BPA in male rats, Environ. Toxicol. Pharmacol. 38 (3) (2014) 1025–1033.
[12] R. Meli, et al., Oxidative stress and BPA toxicity: an antioxidant approach for male and female reproductive dysfunction, Antioxidants 9 (5) (2020).
[13] W.S. Yang, et al., Regulation of ferroptotic cancer cell death by GPX4, Cell 156 (1–2) (2014) 317–331.
[14] Q. Pan, et al., Ferroptosis and liver fibrosis, Int. J. Med. Sci. 18 (15) (2021) 3361–3366.
[15] W. Zeng, et al., The interplay of oncogenic signaling, oxidative stress and ferroptosis in cancer, Int. J. Cancer 153 (5) (2023) 918–931.
[16] X. Fang, et al., The molecular and metabolic landscape of iron and ferroptosis in cardiovascular disease, Nat. Rev. Cardiol. 20 (1) (2023) 7–23.
[17] P. Han, et al., Inhibition of ferroptosis attenuates oligospermia in male Nrf2 knockout mice, Free Radic. Biol. Med. 193 (Pt 1) (2022) 421–429.
[18] M.E.U. Haq, et al., Chronic exposure of bisphenol A impairs carbohydrate and lipid metabolism by altering corresponding enzymatic and metabolic pathways, Environ. Toxicol. Pharmacol. 78 (2020) 103387.
[19] G. Diamante, et al., Systems toxicogenomics of prenatal low-dose BPA exposure on liver metabolic pathways, gut microbiota, and metabolic health in mice, Environ. Int. 146 (2021) 106260.
[20] V.E. Kagan, et al., Oxidized arachidonic and adrenic PEs navigate cells to ferroptosis, Nat. Chem. Biol. 13 (1) (2017) 81–90.
[21] A. Stamenkovic, et al., Oxidized phosphatidylcholines trigger ferroptosis in cardiomyocytes during ischemia-reperfusion injury, Am. J. Physiol. Heart Circ. Physiol. 320 (3) (2021) H1170–H1184.
[22] E.A. Ahmed, D.G. de Rooij, Staging of mouse seminiferous tubule cross-sections, Methods Mol. Biol. 558 (2009) 263–277.
[23] X. Zhou, et al., Polyunsaturated fatty acids metabolism, purine metabolism and inosine as potential independent diagnostic biomarkers for major depressive disorder in children and adolescents, Mol. Psychiatr. 24 (10) (2019) 1478–1488.

[24] C.A. Smith, et al., XCMS: processing mass spectrometry data for metabolite profiling using nonlinear peak alignment, matching, and identification, Anal. Chem. 78 (3) (2006) 779–787.
[25] M. Shi, et al., Prenatal exposure to bisphenol A, E, and S induces transgenerational effects on male reproductive functions in mice, Toxicol. Sci. 172 (2) (2019) 303–315.
[26] L. Li, et al., Bisphenol A induces testicular oxidative stress in mice leading to ferroptosis, Asian J. Androl. 25 (3) (2023) 375–381.
[27] D. Tang, G. Kroemer, Ferroptosis, Curr. Biol. 30 (21) (2020) R1292–R1297.
[28] M.J. Chen, et al., Effect of iron overload on impaired fertility in male patients with transfusion-dependent beta-thalassemia, Pediatr. Res. 83 (3) (2018) 655–661.
[29] B.R. Stockwell, et al., Ferroptosis: a regulated cell death nexus linking metabolism, redox biology, and disease, Cell 171 (2) (2017) 273–285.
[30] V.E. Kagan, et al., Oxidized arachidonic and adrenic PEs navigate cells to ferroptosis, Nat. Chem. Biol. 13 (1) (2017) 81–90.
[31] D. Liang, A.M. Minikes, X. Jiang, Ferroptosis at the intersection of lipid metabolism and cellular signaling, Mol. Cell. 82 (12) (2022) 2215–2227.
[32] J.Y. Lee, et al., Lipid metabolism and ferroptosis, Biology 10 (3) (2021).
[33] G.C. Forcina, S.J. Dixon, GPX4 at the crossroads of lipid homeostasis and ferroptosis, Proteomics 19 (18) (2019).